SCIENTIFIC ARTICLE

Effect of Strain Rates on Failure of Mechanical Properties of Lumbar Intervertebral Disc Under Flexion

Kun Li, PhD[1], Shi-jie Zhang, MS[1], Cheng-fei Du, PhD[2,3], Ji-zhe Zhao, Bachelor[2,3], Qing Liu, PhD[2,3], Chun-qiu Zhang, PhD[2,3], Yan-fang Sun, MS[2,3]

Tianjin Key [1]Laboratory of Film Electronic and Communication Device, [2]Laboratory for Advanced Mechatronic System Design and Intelligent Control and [3]National Demonstration Center for Experimental Mechanical and Electrical Engineering Education, Tianjin University of Technology, Tianjin, China

Objective: To evaluate the strain-rate-dependent viscoelastic properties of the intervertebral disc by *in vitro* experiments.

Method: The biomechanical experiments were conducted from September 2019 to December 2019. The lumbar spines of sheep were purchased within 4–6 hours from the local slaughterhouse, and the intervertebral disc samples were divided into three groups. In rupture group, the samples were used to test the mechanical behavior of the intervertebral disc rupture at different strain rates. In fatigue injury group, the samples were used to test the mechanical behavior of fatigue injury on the intervertebral disc under different strain rates. In internal displacement group, the samples were used to test the internal displacement distribution of the intervertebral disc at different strain rates by applying an optimized digital image correlation (DIC) technique.

Results: Both the yielding and cracking phenomenon occurs at fast and medium loading rates, while only the yielding phenomenon occurs at a slow loading rate. The yield stress, compressive strength, and elastic modulus all increase with the increase of the strain rate, while the yield strain decreases with the increase of the strain rate. The logarithm of the elastic modulus in the intervertebral disc is approximately linear with the logarithm of the strain rate under different strain rates. Both before and after fatigue loading, the stiffness in the loading and unloading curves of the intervertebral disc is inconsistent, forming a hysteresis loop, which is caused by the viscoelastic effect. The strain rate has no significant effect on the internal displacement distribution of the intervertebral disc. Based on the experimental data, the constitutive relationship of the intervertebral disc at different strain rates is obtained. The fitting curves are well coupled with the experimental data, while the fitting parameters are approximately linear with the logarithm of the strain rate.

Conclusions: These experiments indicate that the strain rate has a significant effect on the mechanical behavior of the intervertebral disc rupture and fatigue injury, while the constitutive equation can predict the rate-dependent mechanical behavior of lumbar intervertebral disc under flexion very well. These results have important theoretical guiding significance for preventing lumbar disc herniation in daily life.

Key words: Constitutive model; Fatigue injury; Lumbar disc herniation; Rate-dependent; Viscoelastic

Introduction

Lumbar disc herniation (LDH) is very common clinically, and the pathological basis is lumbar disc degeneration[1].

Lumbar disc herniation is the complete rupture of the annulus fibrosus along with extrusion of the nucleus pulposus. In fact, radial rupture in the annulus fibrosus

may account for 30% to 50% of chronic low back pain cases[2, 3]. The cause of lumbar intervertebral disc herniation is complex, while long-term load accumulation and sudden load mutation are considered to be important causes of herniation. Therefore, it is urgent to analyze the stress/strain behavior of the intervertebral disc under different loading conditions[4, 5].

The intervertebral disc is constructed of the gel-like nucleus pulposus (NP) surrounded by the annulus fibrosus (AF). The annulus fibrosus and nucleus pulposus have the characteristics of cartilage with high water content, so the entire disc displays strong strain-rate-dependent viscoelastic properties that includes maintaining the disc height and absorbing load applied on the spine[6, 7]. Previous biomechanical studies have shown that unflexed segments usually fail through endplate fracture or vertebral compression, while flexion increases the likelihood of the annular fracture, and the exact nature of this rupture depends on the strain rate[8]. Some scholars have conducted a series of in vitro experimental studies to determine how the basic material properties of the intervertebral disc change with the loading rate. For example, Stolworthy et al.[9] performed repeated flexibility tests on the human lumbar intervertebral discs with the use of 11 distinct voluntary loading rates in order to examine rate-dependent viscoelasticity of the intervertebral discs. The results indicated that the flexibility of the spinal segment changed significantly due to the loading rate. Araújo et al.[10] performed quasi-static and dynamic compression tests using porcine intervertebral discs. The quasi-static test was used to obtain the static stiffness coefficient at different strain rates, while the cyclic compression test was used to determine the dynamic stiffness coefficient. Newell et al.[11] performed compression experiments on human intervertebral discs to obtain structural responses, and used reverse finite element techniques to characterize the material properties of intervertebral discs across strain rates. Most of the current studies have observed macroscopic evidence of the rate-related performance in the intervertebral disc, but little is known about the stress and strain of the annulus fibrosus in tissue level, and the control mechanism is not yet clear.

Lumbar disc herniation is usually considered to be a cumulative injury because repeated stress on the annulus fibrosus may cause the nucleus pulposus to penetrate the fibrous ring and eventually extrude posteriorly[12, 13]. Some scholars conducted in vitro experiments to study the effect of fatigue injury on the mechanical properties of the intervertebral disc[14]. For example, Parkinson et al.[15] conducted a

series of in-vitro fatigue tests on the porcine segments to understand the failure mechanism. They concluded that cyclic flexion/ extension bending may lead to disc failure, while larger cyclic compression loads may break the vertebral. Schollum et al.[16] subjected ovine intervertebral discs to 5000 cycles at 0.5 Hz with a peak load corresponding to 30% of that required to achieve failure, then investigated microstructural structural damage in the intervertebral disc subjected to low frequency cyclic loading and flexing. Limited research has studied stress and strain in the intervertebral disc under destructive loading conditions at the tissue level, but these data are crucial to better understand the process of intervertebral disc rupture caused by the annulus fibrosus injury.

The purpose of the present study is to evaluate the mechanical behavior of the intervertebral disc rupture as well as fatigue injury at different strain rates. Simultaneously the internal displacement of the intervertebral disc at different strain rates has also been analyzed. Theoretically, the constitutive relationship of the intervertebral disc at different strain rates is obtained.

Materials and Methods

Sample Preparation

Thirty spines of freshly slaughtered 18-month-old small-tailed Han sheep were purchased within 4–6 hours from the local slaughterhouse. The L_{1-2}, L_{3-4}, L_{5-6} segments were obtained with the intervertebral disc and a small amount of vertebral, removing excess muscle and soft tissue. The test samples were divided into three groups. In rupture group, the test samples from 10 spines were used to test the mechanical behavior of the intervertebral disc rupture at different strain rates. In fatigue injury group, the test samples from 10 spines were used to test the mechanical behavior of fatigue injury on the intervertebral disc under different strain rates. In internal displacement group, the test samples from 10 spines were used to test the internal displacement distribution of the intervertebral disc at different strain rates.

The basic information statistics of the lumbar disc samples are shown in Table 1. The lumbar disc area is $S_{12} = 251 \pm 10$ mm^2, $S_{34} = 310 \pm 10$ mm^2, $S_{56} = 358 \pm 10$ mm^2, and the lumbar disc height is h = 3.98 ± 0.12 mm.
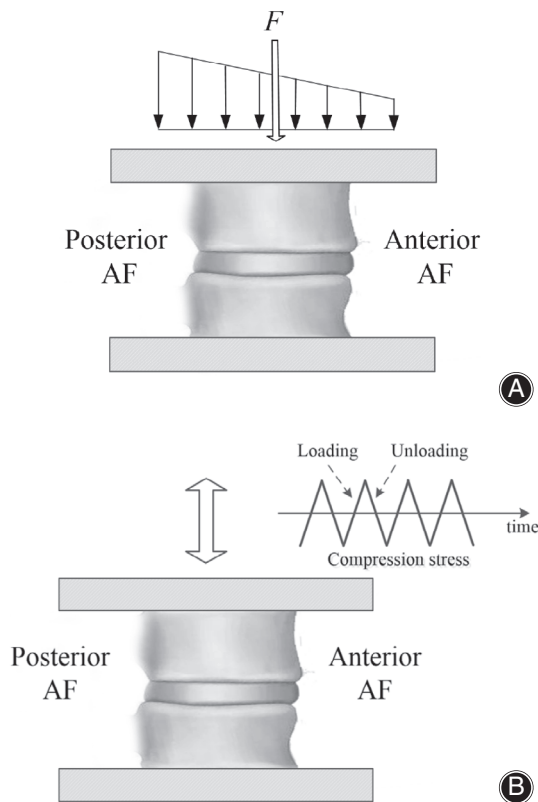
Quasi-static Testing

The experiment was carried out at room temperature (26°C). The intervertebral disc specimen was fixed in forward flexion on the experimental platform through the upper and lower vertebrae, then the compressive loading was applied to the flexed disc (Fig. 1). The WDW-10 computer-controlled electronic universal testing machine was used for quasi-static loading test, while the maximum test load was 10 kN. The EUT-1020 electronic universal fatigue testing machine was used for fatigue loading testing, while the maximum test load is 1 kN and the stroke is ±100 mm (Fig. 2).

1. In rupture group, L_{1-2}, L_{3-4}, and L_{5-6} segments were used for the experiment, and the strain rates were adjusted to

TABLE 1 Statistical table of basic information of lumbar intervertebral disc samples

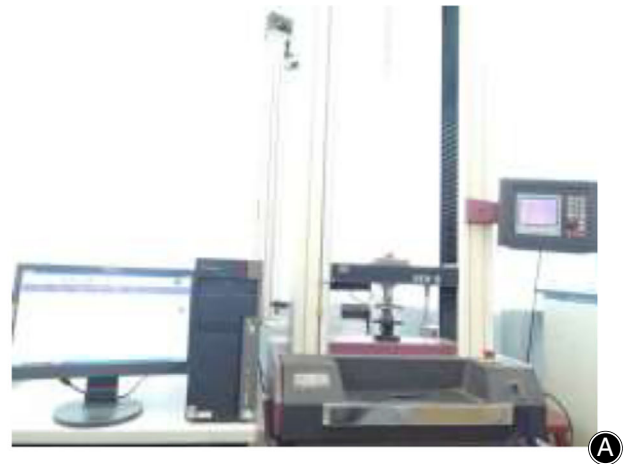| Segments	height(mm)	area(mm^2)
L_{1-2}	3.91	251
L_{3-4}	3.96	310
L_{5-6}	4.01	358

Fig. 1 The experimental methods. The intervertebral disc specimen was fixed in forward flexion on the experimental platform through the upper and lower vertebrae, and the compressive loading was applied to the flexed disc. (A) Quasi-static loading; (B) Fatigue loading.

Fig. 2 The experimental equipment. The WDW-10 computer-controlled electronic universal testing machine was used for quasi-static loading test, and the EUT-1020 electronic universal fatigue testing machine was used for fatigue loading testing. (A) Computer-controlled electronic universal testing machine; (B) Electronic universal fatigue testing machine.

0.0004/s, 0.004/s, and 0.04/s for compression until the lumbar disc rupture.

2. In fatigue injury group, L5-6 segments were used for the experiment, and the strain rates were adjusted to 0.0004/s, 0.004/s, and 0.04/s for compression until the stop displacement of 1.2 mm. Then the samples were unloaded at the same strain rate. The EUT-1020 electronic universal fatigue testing machine was used to cyclically load the samples, with the loading frequency of 1 Hz and the loading cycle of 4000.

3. In internal displacement group, L5-6 segments were used for the experiment, and the strain rates were adjusted to 0.0004/s and 0.004/s for compression until the stop displacement of 1.2 mm.

Mechanical Performance Parameters for Measurement

The stress–strain curve can indirectly reflect the internal damage in the intervertebral disc at different deformation stages. Therefore, the yield point, compressive strength and elastic modulus were determined by the plotting method based on the stress–strain curve.

Yield Point

In the process of tension or compression, when the stress of the material reaches a certain value, there is a sharp increase in strain with a slight increase in stress, and this phenomenon is called yielding. In this study, the yield point was determined by the plotting method based on the stress–strain curve.

Compressive Strength

In the compression test, the maximum compressive stress that the sample bears until disruption or yielding is called the compressive strength. The compressive strength is used to describe the ability of the intervertebral disc that resist compression to avoid failure. In this study, the compressive
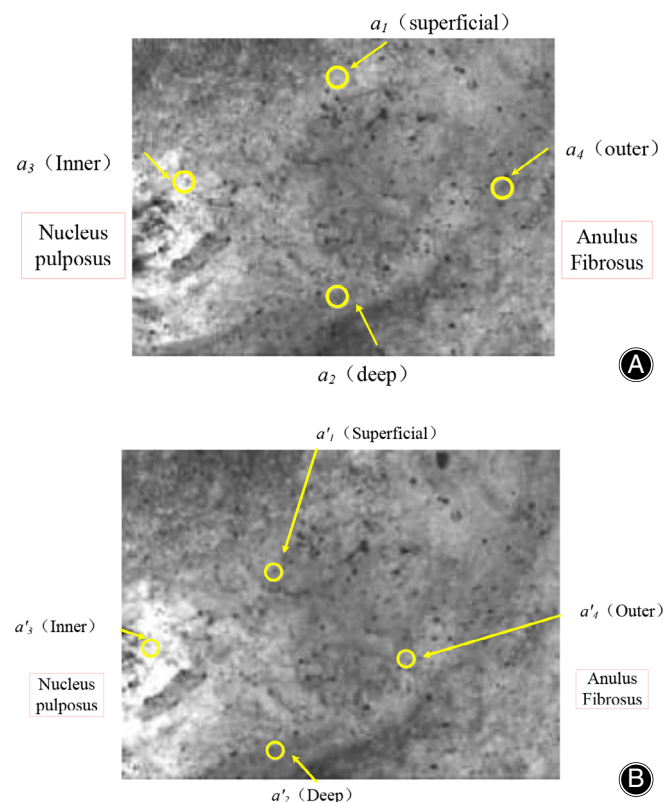
strength was determined based on the maximum stress on the stress–strain curve.

Elastic Modulus

In the stage of elastic deformation, there is a proportional relationship between the stress and strain of the material, while the proportional coefficient is the elastic modulus. The elastic modulus is used to describe the difficulty of elastic deformation in the intervertebral disc. In this study, the elastic modulus was determined based on the linear segment of the initial deformation on the stress–strain curve.

Internal Displacement for Measurement

The DIC technology[17] was used to track the marked points, and the deformation in different regions of the intervertebral disc was calculated. Figure 3 shows the collected images in posterior AF of the intervertebral disc before and after quasi-static loading, and the evenly distributed black spots are the iron oxide nanoparticles. A set of marked points $a1$ $(x1, y1)$ and $a2$ $(x2, y2)$ are selected with similar x values, and the change of axial displacement distribution is reflected by comparing the change of y values before and after quasi-static loading. A set of marked points $a3$ $(x3, y3)$ and $a4$ $(x4, y4)$ are selected with similar y values, and the change of radial displacement distribution is reflected by comparing the change of x values before and after quasi-static loading.

Statistical Analysis

A one-way analysis of variance (ANOVA) with repeated measures was performed to detect the differences among the experimentally measured values of the mechanical performance parameters as well as the internal displacement in the compression tests. Statistical significance was accepted for pb0.05. Data points in the figures represent mean values, whereas error bars indicate the standard errors above and below corresponding mean values.

Result

Mechanical Behavior of the Intervertebral Disc Rupture at Different Strain Rates

Figure 4 shows the mechanical behavior of the intervertebral disc rupture at different strain rates. The results show that both the yielding and cracking phenomenon occur at fast and medium loading rates, while only the yielding phenomenon occurs at slow loading rates.

① The stress–strain curve generally exhibits three-segment characteristics at the strain rate of 0.0004/s: toe segment, linear segment, yield and strain softening segment.
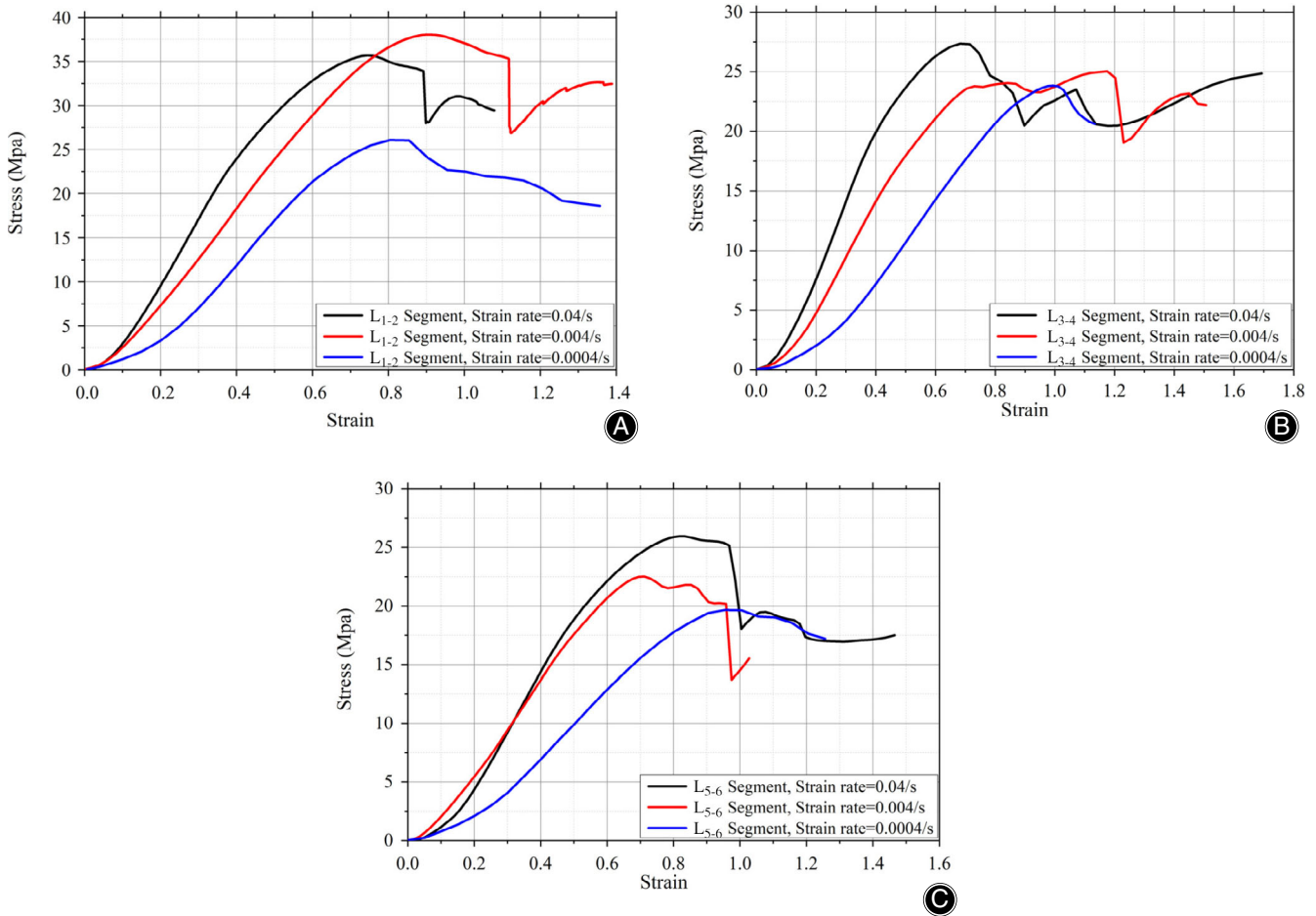
② The stress–strain curve generally exhibits multi-segment characteristics at the strain rate of 0.004/s and 0.04/s: toe segment, linear segment, yield and strain softening segment, failure segment.

Based on the stress–strain curve as shown in Fig. 4, mechanical performance is determined and listed in Table 2. The results show that the yield stress, compressive strength and elastic modulus all increase with the increase of the strain rate, while the yield strain decreases with the increase of the strain rate. It can be seen that the intervertebral disc has significant rate-dependent characteristics. In addition, the mechanical properties of the intervertebral discs are different between different segments, and the elastic modulus changes as follow: L_{5-6} segment $<L_{3-4}$ segment $<L_{1-2}$ segment.

Figure 5 shows the correlation between the elastic modulus of the intervertebral disc and the strain rate. It can be concluded from the experimental data that the logarithm of the elastic modulus in the intervertebral disc is approximately linear with the logarithm of the strain rate.

Mechanical Behavior of Fatigue Injury on the Intervertebral Disc Under Different Strain Rates

A comprehensive study of the complete process of loading–unloading is helpful to determine the different constitutive properties of the intervertebral disc (nonlinear elastic or nonlinear viscoelastic). Figure 6 shows the loading–unloading curves of L_{5-6} segment of the intervertebral disc at different strain rates before and after fatigue loading. The results show that the intervertebral discs exhibit nonlinear stress–strain

Fig. 3 The collected images in posterior AF of the intervertebral disc by the DIC technology. The evenly distributed black spots are the iron oxide nanoparticles, and the DIC technology was used to track the marked points. (A) The collected images before quasi-static loading; (B) The collected images after quasi-static loading.

STRAIN RATES ON INTERVERTEBRAL DISC

Fig. 4 Stress–strain characteristic curve of the intervertebral disc at different strain rates. Both the yielding and cracking phenomenon occur at fast and medium loading rates, while only the yielding phenomenon occurs at slow loading rates. (A) The mechanical behavior in L_{1-2} Segment; (B) The mechanical behavior in L_{3-4} Segment; (C) The mechanical behavior in L_{5-6} Segment.

TABLE 2 Mechanical performance parameters of the intervertebral disc under different strain rates

| Segments	Strain rate	Yield stress(MPa)	Yield strain	Compression strength(MPa)	Elastic modulus(MPa)
L_{1-2}	0.0004	29.9	0.77	26.1	49.25
	0.004	40	0.79	38.0	55.45
	0.04	38.7	0.59	35.8	74.85
L_{3-4}	0.0004	26.5	0.95	23.9	34.67
	0.004	26.9	0.67	23.9	47.14
	0.04	33.5	0.6	27.4	65
L_{5-6}	0.0004	21	0.88	19.7	29.44
	0.004	23.9	0.64	22.5	42.74
	0.04	27.4	0.65	26	51.8

characteristics at different loading rates ($P < 0.05$). The stiffness of the loading and unloading curves is inconsistent, forming a hysteresis loop, which is caused by the viscoelastic effect.

Based on the stress–strain characteristic curve shown in Fig. 6, the elastic modulus of the linear segment is calculated and listed in Table 3. The results show that after fatigue loading, the elastic modulus of L_{5-6} segment increases significantly.

In addition, the elastic modulus gradually increases as the strain rate increases, with a significant rate correlation.
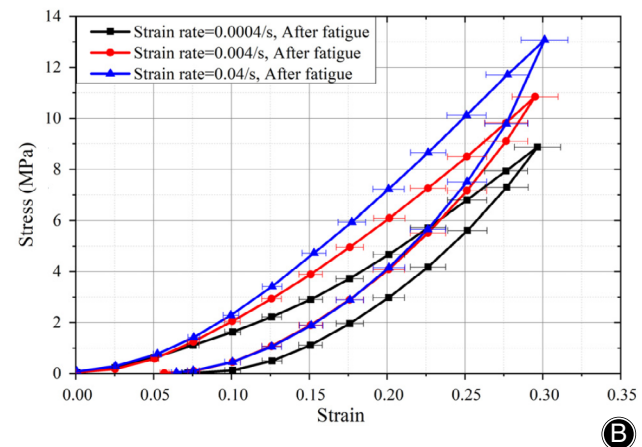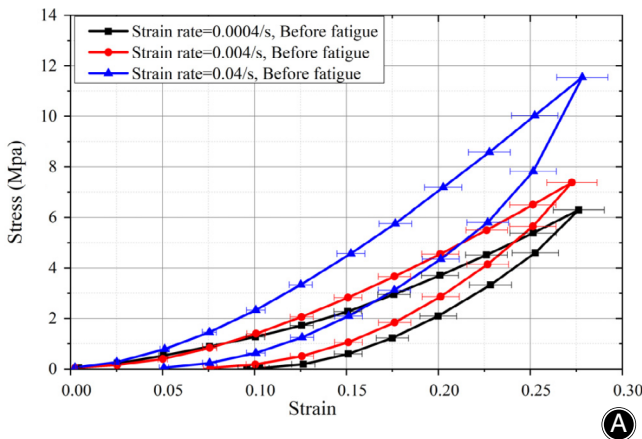
Internal Displacement Distribution of the Intervertebral Disc at Different Strain Rates
Figure 7 shows the axial displacement distribution inside the flexed intervertebral disc which was applied with
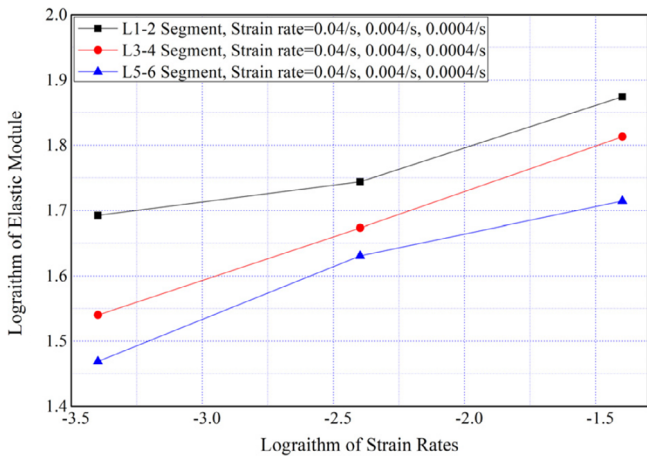
Fig. 5 Strain rate dependence of the elastic modulus. The experimental data shows that the logarithm of the elastic modulus in the intervertebral disc is approximately linear with the logarithm of the strain rate.

TABLE 3 Mechanical properties of the intervertebral disc before and after fatigue			
Segments	Status	Strain rate	Elastic modulus (MPa)
L_5-L_6	Before fatigue	0.0004	29.80
		0.004	33.08
		0.04	54.99
	After fatigue	0.0004	41.62
		0.004	48.28
		0.04	54.14

Fig. 6 Loading–unloading curves of the intervertebral disc at different strain rates. The stiffness of the loading and unloading curves is inconsistent, forming a hysteresis loop, which is caused by the viscoelastic effect. (A) Loading–unloading curves before fatigue; (B) Loading–unloading curves after fatigue.
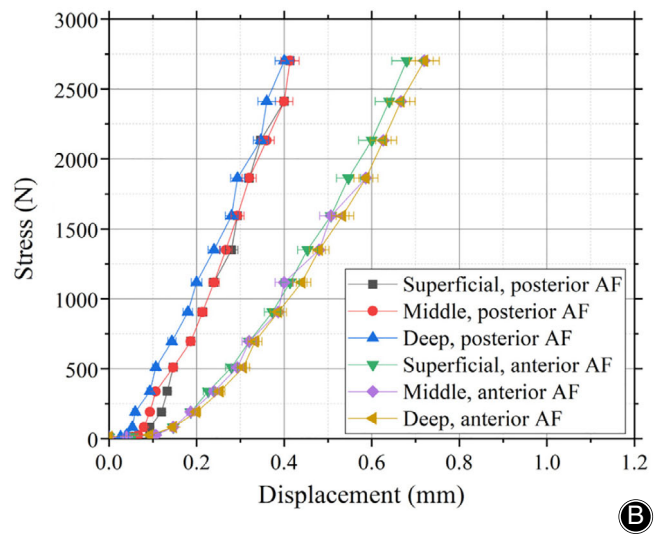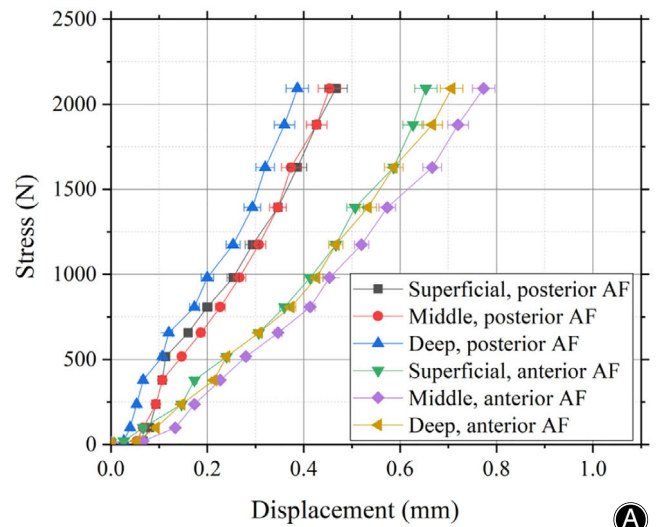
Fig. 7 Axial displacement distribution. The strain rate has no significant effect on the axial displacement distribution inside the intervertebral disc. Overall, posterior AF exhibited smaller axial displacement than anterior AF. (A) Axial displacement distribution at strain rate of 0.0004/s; (B) Axial displacement distribution at strain rate of 0.004/s.
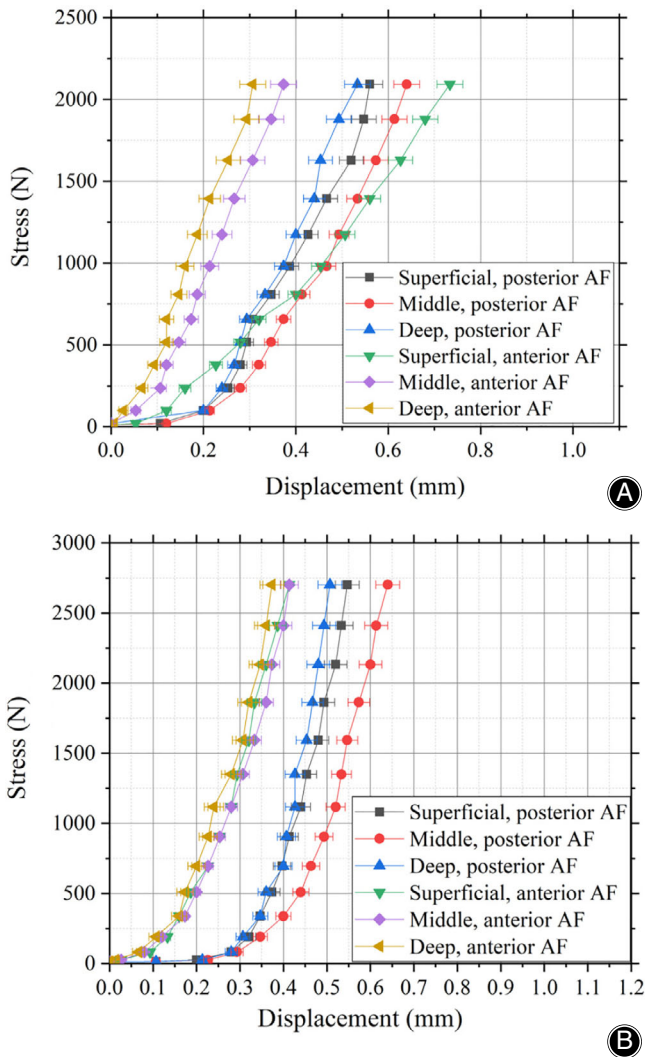
Fig. 8 Radial displacement distribution. The strain rate has no significant effect on the radial displacement distribution inside the intervertebral disc. Overall, posterior AF exhibited greater radial displacement than anterior AF. (A) Radial displacement distribution at strain rate of 0.0004/s; (B) Radial displacement distribution at strain rate of 0.004/s.

compressive loading ($P < 0.05$). It can be seen that the strain rate has no significant effect on the axial displacement distribution inside the intervertebral disc. Overall, posterior AF exhibited smaller axial displacement than anterior AF.

Figure 8 shows the radial displacement distribution inside the flexed intervertebral disc which was applied with compressive loading ($P < 0.05$). It can be seen that the strain rate has no significant effect on the radial displacement distribution inside the intervertebral disc. Overall, posterior AF exhibited greater radial displacement than anterior AF. For the posterior region, the radial displacement is largest in the middle layer and smallest in the outer layer. For the anterior region, the radial displacement is minimal in the inner layer.

Rate-dependent Constitutive Relationship of the Intervertebral Disc

In order to study the mechanical properties of the intervertebral disc at different strain rates, the following equation is used to describe the constitutive relationship of the intervertebral disc:

$$\sigma = E_1\varepsilon^3 + E_2\varepsilon^2 + E_3\varepsilon \qquad (1)$$

Based on the linear segment of the stress–strain curve in Fig. 4, the constitutive relationship of the intervertebral disc at different strain rates is obtained, as shown in Fig. 9. This figure shows that the fitting curve is well coupled with the experimental curve, indicating that the constitutive equation can well represent the stress–strain relationship of the flexed intervertebral disc at different strain rates.

The fitting parameters at different strain rates are as follows: when the loading rate is 0.0004, $E_1 = -38.721$, $E_2 = 67.433$, $E_3 = -3.1688$. When the loading rate is 0.004, $E_1 = -174.8$, $E_2 = 163.37$, $E_3 = -2.2938$. When the loading rate is 0.04, $E_1 = -314.8$, $E_2 = 248.45$, $E_3 = 0.7319$. From the experimental data, it can be ascertained that the fitting parameters are approximately linear with the logarithm of the strain rate (Fig. 10).

Discussion

The purpose of the present study is to evaluate the mechanical behavior of the intervertebral disc rupture as well as fatigue injury at different strain rates. Simultaneously the internal displacement of the intervertebral disc at different strain rates has also been analyzed. Theoretically, the constitutive relationship of the intervertebral disc at different strain rates is obtained.

Stress–strain Curve

Both the yielding and cracking phenomenon occurs at fast and medium loading rates, while only the yielding phenomenon occurs at slow loading rates. This is consistent with the research results of Veres et al.[18], who used nuclear pressurization to transmit sudden pressure impulses to the nucleus pulposus in both neutrally positioned and flexed intervertebral discs. Experimental results showed that the internal morphology of the intervertebral disc disruptions caused by high rate pulse loading is significantly different from that caused by gradual low rate loading. These morphological differences indicate that the internal failure mechanism of the intervertebral disc changes with the loading rate.

Mechanical Performance Parameters

The yield stress, compressive strength, and elastic modulus all increase with the increase of the strain rate, while the yield strain decreases with the increase of the strain rate. The logarithm of the elastic modulus in the intervertebral disc is approximately linear with the logarithm of the strain rate under different strain rates. This is consistent with the
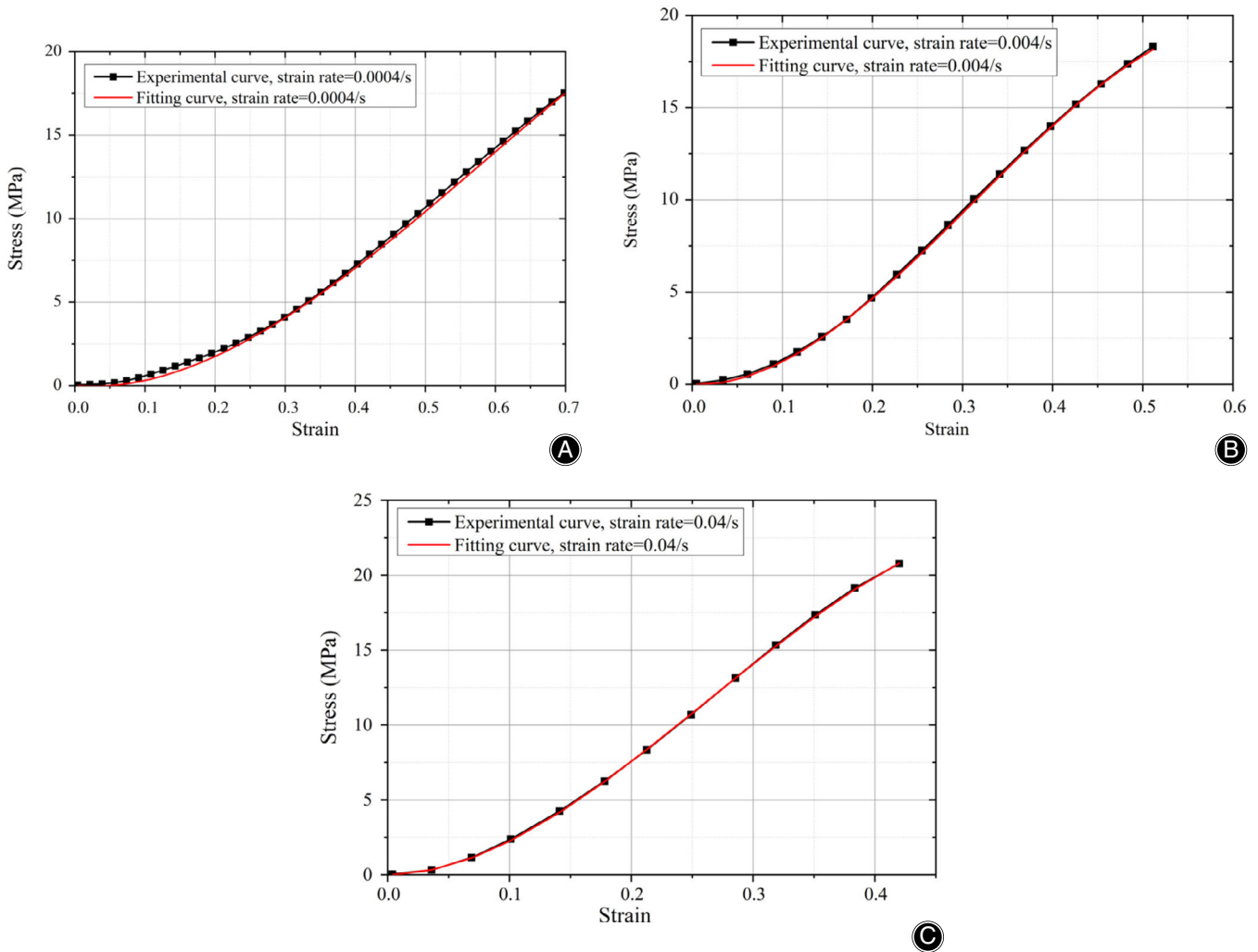
Fig. 9 Stress–strain fitting curve. The fitting curve is well coupled with the experimental curve, indicating that the constitutive equation can well represent the stress–strain relationship of the flexed intervertebral disc at different strain rates. (A) The fitting curve at strain rate of 0.0004/s; (B) The fitting curve at strain rate of 0.004/s; (C) The fitting curve at strain rate of 0.04/s.

research results of Newell *et al.*[19], who applied uniaxial compression to the bovine lumbar intervertebral discs, and input experimental data into an inverse finite element modeling optimisation algorithm to obtain the material properties of the intervertebral disc across strain rates. On this basis, the correlation between the elastic modulus of the intervertebral disc and the strain rate ˙ was derived.

Mechanical Properties Between Different Segments
The mechanical properties of the intervertebral discs are different between different segments, and the elastic modulus changes as follow: L_{5-6} segment < L_{3-4} segment < L_{1-2} segment. This is consistent with the findings of Causa *et al.*[20], who investigated the influence of the spatial location and structural components on the mechanical properties of porcine intervertebral disc. L_{2-3} segment showed a higher elastic modulus value with lower load at rupture. On the contrary,

L_{4-5} segment showed a lower elastic modulus value with higher load at rupture.

Figure 11 is the force analysis of the lumbar spine when the human body bends to lift a heavy object, where θ is the forward flexion angle, F_N is the pressure on the spine. F_e is the extensor force, a is the arm of F_e; W_1 is the gravity of the object, b is the arm of W_1; W is the upper body gravity of the human, and c is the arm of W.

When the human body is leaning forward, the back muscles will provide strong pulling force to maintain the torque balance of the lumbar spine. According to the moment balance, the extensor force can be calculated:

$$F_e = (W_1 b + Wc)/a \qquad (2)$$

Based on the force balance, the pressure in the spine can be calculated:
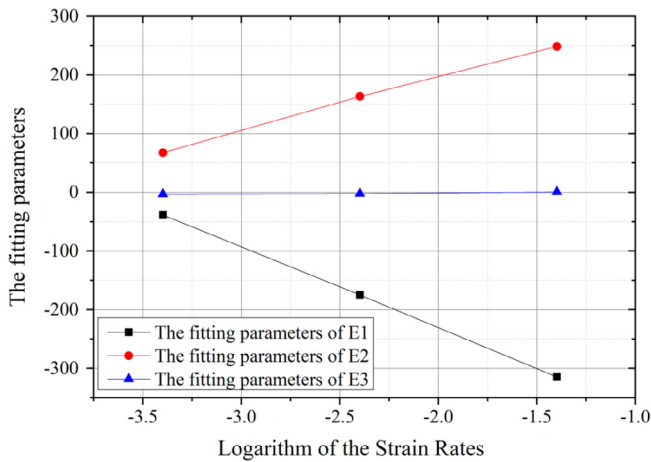
Fig. 10 Strain rate dependence of the fitting parameters. The experimental data shows that the fitting parameters are approximately linear with the logarithm of the strain rate.
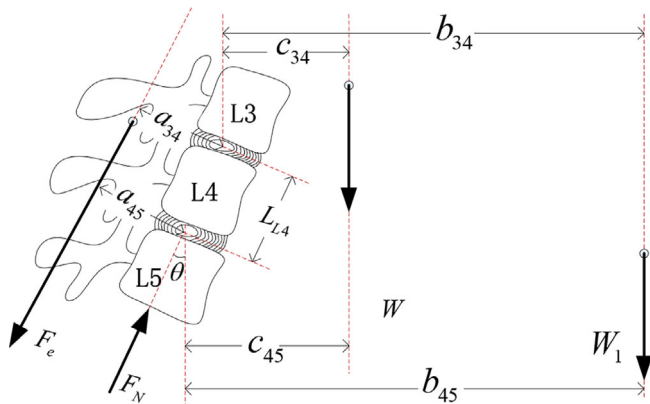

Fig. 11 Force analysis of the lumbar spine when the human body bends over to lift weights. When the human body bends to lift heavy objects, some slight movements will cause the L5-6 segment to bear huge pressure, which will cause some patients' lumbar intervertebral discs to be damaged, and lumbar disc herniation occurs mostly in this segment.

$$F_N = F_e + (W + W_1)\cos\theta \qquad (3)$$

Based on formulas (2)–(3), the pressure in the lumbar intervertebral disc when the human body bends to lift a weight can be calculated, as shown in Table 4. The results show that if the human body carries a 200 N weight and only flexes forward by 10°, the pressure F_N in the lumbar intervertebral disc can increase to several times the body weight. In particular, the pressure in the $L_{5\text{-}6}$ segment is the largest. When the human body bends to lift heavy objects, some slight movements will cause the $L_{5\text{-}6}$ segment to bear huge pressure, which will cause some patients' lumbar intervertebral discs to be damaged, and lumbar disc herniation occurs mostly in this segment.

TABLE 4 Stress of the lumbar intervertebral disc when the human body bends to lift heavy objects

Flexion angle	Weight(N)	Segments	Extensor force (N)	Pressure on the spine (N)
10°	200	L1-L2	3000	3711
		L3-L4	3243	3954
		L5-L6	3365	4075
	500	L1-L2	6000	7015
		L3-L4	6347	7363
		L5-L6	6521	7536
30°	200	L1-L2	3000	3808
		L3-L4	3700	4508
		L5-L6	4050	4858
	500	L1-L2	6000	7155
		L3-L4	7000	8155
		L5-L6	7500	8655

Fatigue Injury

Both before and after fatigue loading, the stiffness of the loading and unloading curve is inconsistent, forming a hysteresis loop, which is caused by the viscoelastic effect[7]. This is consistent with the results of Race et al.[21], who applied compressive axial load to the intervertebral disc, to quantify the effects of hydration and loading rate on the mechanical response of the intervertebral disc. Experimental results showed that intervertebral disc compressive mechanical properties were significantly dependent on loading rate and hydration.

In addition, the elastic modulus increased significantly after fatigue loading. This result is consistent with the research by Parkinson et al.[15], who conducted a series of in-vitro fatigue tests on the porcine lumbar intervertebral disc to understand its injury mechanism. Experimental results showed that cyclic flexion/extension bending is more likely to cause the intervertebral disc injury, while large cyclic compressive loading is more likely to cause the vertebral fracture. When the intervertebral disc is subjected to a long-term great level of axial load, the water will be squeezed out of the intervertebral disc, so the height of the intervertebral disc decreases and lumbar disc herniation occurs[16]. Therefore, in order to avoid lumbar disc herniation, more functional exercises on the lower back muscles should be performed to control weight, avoid lifting heavy weights, and avoid maintaining a bad posture for a long time. After working continuously for a period of time, the human body should take appropriate rest to avoid lumbar disc pain caused by continued strong pressure[22].

Internal Displacement Distribution

The strain rate has no significant effect on the axial displacement distribution inside the intervertebral disc. Overall, posterior AF exhibited smaller axial displacement and greater radial displacement than anterior AF. This is consistent with the results of Qasim et al.[23], who refined the finite element model of lumbar intervertebral disc to investigate the

initiation and progression of mechanical damage in the intervertebral disc under different cyclic loading conditions. Simulation results showed that, the damage accumulated preferentially in the posterior region of the intervertebral disc under all loading conditions. When compressive loading was applied to a flexed intervertebral disc, there was an anteroposterior pressure gradient due to compression of the fluid nucleus, and the annular distortions could be formed[24, 25].

In addition, for the posterior region, the radial displacement is largest in the middle layer and smallest in the outer layer. For the anterior region, the radial displacement is minimal in the inner layer. This is consistent with the research results of Wade et al.[26], who compressed healthy ovine lumbar intervertebral disc to failure in either a neutral posture or in high physiological flexion in order to provide the microstructural investigation of compression-induced disruption of the flexed lumbar disc. Experimental results showed that damage was initiated in the mid- then outer annular fibers; this a likely consequence of the higher strain burden in these same fibers arising from endplate curvature.

Limitation of the Study
In this paper, the constitutive relationship of the intervertebral disc at different strain rates is obtained based on the experimental data. The fitting curves are well coupled with the experimental data, while the fitting parameters are approximately linear with the logarithm of the strain rate. However, the shortcoming is that the linear equation has not been obtained to describe the linear relationship between the fitting parameters and the logarithm of the strain rate.

Conclusion
In this paper, quasi-static compressive loading was applied to the flexed intervertebral discs at different strain rates. Mechanical properties were determined based on the stress–strain curves. Simultaneously the optimized digital image correlation technique was applied to analyze the mechanical properties in different regions of the intervertebral disc. Experimental results showed that the strain rate has a significant effect on the mechanical behavior of the intervertebral disc rupture and fatigue injury, while the constitutive equation can be used to predict the rate-dependent mechanical behavior of lumbar intervertebral disc under flexion. The research work in this article has important theoretical guiding significance for preventing lumbar disc herniation in daily life.

References

1. Oster BA, Kikanloo SR, Levine NL, Lian J, Cho W. Systematic review of outcomes following 10-year mark of spine patient outcomes research trial (SPORT) for degenerative Spondylolisthesis. Spine (Phila Pa 1976), 2020, 45: 820–824.
2. Pavlović T, Štefančić K, Rožanković M, et al. Ventrolateral disc herniation causes psoas muscle compression: a case report. Radiol Case Rep, 2019, 15: 136–140.
3. Sapiee NH, Thambyah A, Robertson PA, Broom ND. New evidence for structural integration across the cartilage-vertebral endplate junction and its relation to herniation. Spine J, 2019, 19: 532–544.
4. Zhang CQ, Zhang T, Gao L, et al. Ratcheting behavior of intervertebral discs under cyclic compression: experiment and prediction. Orthop Surg, 2019, 11: 895–902.
5. Meng Z, Wang C, Tian LJ, Zhang XJ, Guo D, Zou Y. Pressure distributions inside intervertebral discs under unilateral pedicle screw fixation in a porcine spine model. J Orthop Surg Res, 2018, 13: 254.
6. Beekmans SV, Emanuel KS, Smit TH, Iannuzzi D. Stiffening of the nucleus pulposus upon axial loading of the intervertebral disc: An experimental in situ study. JOR Spine, 2018, 1: e1005.
7. Newman HR, Bowles RD, Buckley MR. Viscoelastic heating of insulated bovine intervertebral disc. JOR Spine, 2018, 1: e1002.
8. Wade KR, Schollum ML, Robertson PA, Thambyah A, Broom ND. A more realistic disc herniation model incorporating compression, flexion and facet-constrained shear: a mechanical and microstructural analysis. Part I: low rate loading. Eur Spine J, 2017, 26: 2616–2628.
9. Stolworthy DK, Zirbel SA, Howell LL, Samuels M, Bowden AE. Characterization and prediction of rate-dependent flexibility in lumbar spine biomechanics at room and body temperature. Spine J, 2014, 14: 789–798.
10. Araújo ÂR, Peixinho N, Pinho AC, Claro JC. Quasi-static and dynamic properties of the intervertebral disc: experimental study and model parameter determination for the porcine lumbar motion segment. Acta Bioeng Biomech, 2015, 17: 59–66.
11. Newell N, Carpanen D, Grigoriadis G, Little JP, Masouros SD. Material properties of human lumbar intervertebral discs across strain rates. Spine J, 2019, 19: 2013–2024.
12. Gregory DE, Callaghan JP. An examination of the influence of strain rate on subfailure mechanical properties of the annulus fibrosus. J Biomech Eng, 2010, 132: 091010.
13. Qasim M, Natarajan RN, An HS, Andersson GB. Damage accumulation location under cyclic loading in the lumbar disc shifts from inner annulus lamellae to peripheral annulus with increasing disc degeneration. J Biomech, 2014, 47: 24–31.
14. Berger-Roscher N, Casaroli G, Rasche V, Villa T, Galbusera F, Wilke HJ. Influence of complex loading conditions on intervertebral disc failure. Spine (Phila Pa 1976), 2017, 42: E78–E85.
15. Parkinson RJ, Callaghan JP. The role of dynamic flexion in spine injury is altered by increasing dynamic load magnitude. Clin Biomech, 2009, 24: 148–154.
16. Schollum ML, Wade KR, Robertson PA, Thambyah A, Broom ND. A microstructural investigation of disc disruption induced by low frequency cyclic loading. Spine (Phila Pa 1976), 2018, 43: E132–E142.
17. Gao LL, Qin XY, Zhang CQ, Gao H, Ge HY, Zhang XZ. Ratcheting behavior of articular cartilage under cyclic unconfined compression. Mater Sci Eng, 2015, 57: 371–377.
18. Veres SP, Robertson PA, Broom ND. ISSLS prize winner: how loading rate influences disc failure mechanics a microstructural assessment of internal disruption. Spine (Phila Pa 1976), 2010, 35: 1897–1908.
19. Newell N, Grigoriadis G, Christou A, Carpanen D, Masouros SD. Material properties of bovine intervertebral discs across strain rates. J Mech Behav Biomed Mater, 2017, 65: 824–830.
20. Causa F, Manto L, Borzacchiello A, et al. Spatial and structural dependence of mechanical properties of porcine intervertebral disc. J Mater Ence Mater Med, 2002, 13: 1277–1280.
21. Race A, Broom ND, Robertson P. Effect of loading rate and hydration on the mechanical properties of the disc. Spine (Phila Pa 1976), 2000, 25: 662–669.
22. Vergroesen PP, van der Veen AJ, van Royen BJ, Kingma I, Smit TH. Intradiscal pressure depends on recent loading and correlates with disc height and compressive stiffness. Eur Spine J, 2014, 23: 2359–2368.
23. Qasim M, Natarajan RN, An HS, Andersson GB. Initiation and progression of mechanical damage in the intervertebral disc under cyclic loading using continuum damage mechanics methodology: a finite element study. J Biomech, 2012, 45: 1934–1940.
24. Nawathe S, Yang H, Fields AJ, Bouxsein ML, Keaveny TM. Theoretical effects of fully ductile versus fully brittle behaviors of bone tissue on the strength of the human proximal femur and vertebral body. J Biomech, 2015, 48: 1264–1269.
25. Yang H, Jekir MG, Davis MW, Keaveny TM. Effective modulus of the human intervertebral disc and its effect on vertebral bone stress. J Biomech, 2016, 49: 1134–1140.
26. Wade KR, Robertson PA, Thambyah A, Broom ND. How healthy discs herniate: a biomechanical and microstructural study investigating the combined effects of compression rate and flexion. Spine (Phila Pa 1976), 2014, 39: 1018–1028.